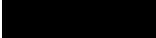
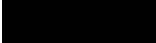
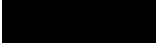
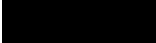



The Effects of Orifice Configurations on the Spray Cone of a Pintle Injector

Group #26

By:

Sean Cornish	(USCID: )
Zachary Fujita	(USCID: )
Mark McDermott	(USCID: )
Michael Smat	(USCID: )
Patrick Trunfio	(USCID: )

Presented to:

Dr. Charles Radovich, Dr. Yann Staelens, Dr. Akshay Potnuru, Dr. Robert Antypas

AME 441aL Senior Projects Laboratory

3 September 2021

ABSTRACT

Pintle injectors are used in bipropellant rocket engines to atomize and mix propellants for efficient combustion during engine use. Design of an effective injector requires relations gathered from classical physics, empirical research, and testing with hardware. One geometric relation that has not been characterized in prior research is the effect of multiple orifice rows on the injection characteristics of a pintle, namely its spray cone angle, mass flow distribution, and mixing. This research will evaluate the effect that two rows of pintle orifices have on these injection parameters as the distance between the rows varies by performing water flow testing on a pintle injector. To provide results informative for other designs, tests of each orifice row spacing configuration will be conducted at various radial to axial flow momentum ratios. A catch basin subdivided over a range of spray cone angles will be fitted to a water flow test stand developed by the Rocket Propulsion Laboratory at USC. Measuring the weight of water captured in each basin sector can be used to determine how mass flow distribution by orifice rows. Use of a dye in one of the water flows will allow assessment of propellant mixing throughout the spray cone. The data collected will be used to create empirical correlations showing how the spray cone angle, momentum distribution, and mixing of a pintle varies with the distance between its stacked rows, which can then be used to increase the mass flow capacity.

I. INTRODUCTION

A pintle is an injector type for liquid rocket engines that features a single, central injection element protruding into the chamber [1]. One propellant flows through this central element, known as the pintle, and is injected in the radial direction into the chamber by discrete orifices or a continuous annulus, while the other is injected in the axial direction around the pintle circumference, as seen in Figure 1.

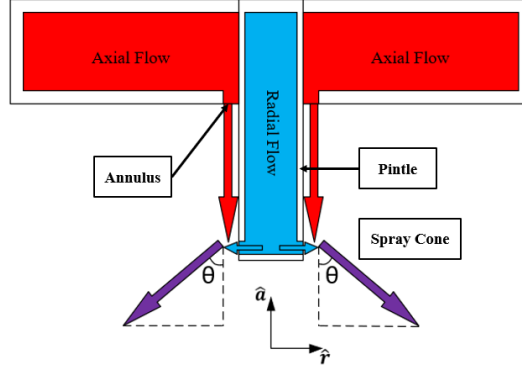


Figure 1. Schematic of the axial and radial flows produced by a pintle injector, illustrating the axial (\hat{a}) and radial (\hat{r}) directions.

The axial and radial flows indicated above can be either fuel or oxidizer, depending on the design. The spray cone (purple arrows) propagates at the spray cone angle (θ) into the combustion chamber.

Orifice and annulus dimensions and geometry affect the collision of the propellants near the pintle tip, which forms a mixed propellant sheet known as the spray cone, illustrated with purple arrows in Figure 1,

The spray cone of a pintle injector must be optimized during the design process to manage flow and energy distribution throughout the chamber, affecting combustion efficiency [2], combustion instability [3], and thermal loads [4]. Due to the complex multi-phase fluid dynamics that characterize propellant mixing, spray cone behavior is typically determined from empirical relations found in research or individual injector testing. While individual injector testing is ultimately a necessary validation step [5], utilizing empirical relations from existing studies first decreases the number of prototyped design iterations, saving time and money [6].

This project will investigate the effect of multiple rows of pintle orifices on the spray cone angle and mass flow distribution into the chamber. Stacking rows of orifices on the pintle, as shown in Figure 2, allows for a greater mass flow rate at a given injector and orifice size. This allows for greater thrust for a smaller engine, increasing the lift-to-weight ratio of the engine. While extensive research has investigated the effect of the ratio of momentum of propellant flowing radially to propellant flowing axially on the spray cone angle [7] [8] [9] [10] [11], less research has focused on discrete orifices and none on multiple rows of orifices, despite the existence of successful engine designs employing multiple rows [12].

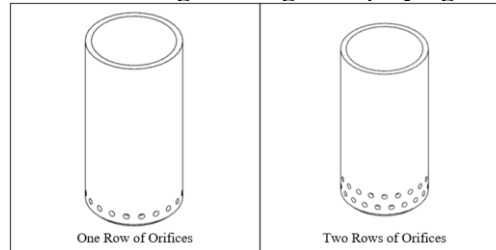


Figure 2. Examples of pintles with multiple stacked rows of orifices

Moreover, work to characterize the distribution of propellant in the spray from the pintle is limited, with spray results reported as a single angle rather than a range. This is of particular concern for pintle injectors employing discrete radial orifices rather than a pintle annulus, since the concentrated radial momentum can produce a larger cone angle locally in the combined spray that can impact the wall before the total momentum ratio would predict [2] [13]. Impingement of unmixed flow on the chamber wall

decreases combustion efficiency [2] [14]. Evaluating the flow mixing in a pintle injector after the collision point has also not been directly studied. Even mixing improves combustion efficiency by ensuring the maximum propellant mass is consumed in combustion [15]. Therefore, expanding the current understanding of the effect of momentum ratio on mass flow distribution for pintle injectors with discrete orifices is critical to design injector geometry to provide the optimal flow pattern in the combustion chamber.

Assessment of injector behavior will begin with hand calculations based on analytical approaches and previous research. While none of the literature focuses on this question specifically, each paper presents information about models used to predict the behavior of the fluid interactions that occur during this type of injection. A water flow test stand will evaluate the flow produced by pintle injectors with varying hole row spacing over a range of injected flow momentums for spray cone angle, spray cone mass flow distribution, and mixing performance. These results will be used to inform a new spray cone model that may combine or modify existing spray cone models or introduce a correction factor to describe spray cone phenomena in a pintle engine based on the geometric parameters of multiple orifice rows.

II. THEORY

A. GEOMETRY AND FLOW CHARACTERIZATION

While the pintle injector configuration offers significant design flexibility, certain geometric parameters are generally maintained. One geometric parameter, blockage factor, evaluates distribution of radial momentum in discrete orifices rather than a continuous annulus in the pintle [7] [9]. The blockage factor describes the fraction of the pintle circumference occupied by radial orifices as

$$BF = \frac{Nd}{\pi d_p} \quad (1)$$

where N is the number of orifices, d is the width of the orifice, and d_p is the outer diameter of the pintle [1]. Typical blockage factor values range from 0.3 to 0.5 [1] [7] [9]. Although a continuous annulus is common, and would compute a blockage factor of 1, BF between 0.5 and 1 is less common because of the structural and manufacturing challenges of producing more orifices with increasingly narrow walls separating the orifices.

Another geometric parameter, known as skip distance (D_S), nondimensionalizes the distance the axial flow travels before impacting the radial flow according to

$$D_S = L_S/D_P \quad (2)$$

where L_S is the axial distance traveled and D_P is the pintle diameter [1]. At a greater L_S , the flow in the axial direction may diffuse more into the chamber, changing the momentum distribution in the collision [3] and even the discharge behavior of the radial orifices in the pintle because of changes to the orifice outlet pressure [13]. An optimal D_S of 1 has been proposed from measurements of combustion efficiency over a range of D_S [16].

Although this study does not focus on the breakup of the liquid sheet, the multiphase flow regime may affect the spray cone angle and distribution. Estimation of the breakup of the sheet is also necessary to assess the engine combustion performance for injector sizing, since this injector was designed for an engine meeting a set of parameters described in the Experimental Setup section, and to determine the placement of the measurement apparatus for this experiment. The Weber number is a nondimensional quantity used to describe the ratio of fluid inertia to fluid cohesion to inform breakup estimations, and is defined as

$$We = \frac{\rho v^2 L}{\sigma} \quad (3)$$

where L is a characteristic length scale, typically chosen as the orifice diameter, v is the fluid velocity, and σ is the surface tension. Depending on the phenomena described, the density ρ can refer either to the liquid [17] [18] or the surrounding gas [11] [12] [19]. The Weber number can be used as a defining parameter in gas-liquid pintle injectors [10] [14] [20]. For liquid-liquid injector types, the liquid density is used [7] [20], as it will be in this study, to perform sizing and setup calculations.

B. SPRAY CONE BEHAVIOR

Many empirical studies have investigated the effect of propellant injection momentum on performance by evaluating the combined behavior of the axial and radial flows. These flow momentums are nondimensionalized in the total momentum ratio (TMR) [9], defined as

$$TMR = \frac{\dot{m}_r v_r}{\dot{m}_a v_a} \quad (4)$$

Because of the spray cone angle is formed by a collision between two moving continua, TMR is strongly related to the spray cone angle. Assuming a perfectly inelastic collision, the spray cone angle θ would be defined by

$$TMR = \tan \theta \quad (5)$$

However, (3) does not accurately describe the momentum characteristics of most pintle injectors [1] [7] [8]. Consequently, numerous studies have related the development of the spray cone to other parameters of the injector. Some models predict spray cone angle by considering blockage factor in the momentum ratio: the local momentum ratio (LMR) by considering the momentum of the flows only at the radial orifices according to

$$LMR = \frac{\dot{m}_r v_r}{\frac{d}{w} \dot{m}_a v_a} \quad (6)$$

where d is the diameter or width of the radial jet and w is the width of the sector of the axial sheet of the orifice's circumferential pattern [13].

A summary of the proposed models to relate spray cone angle to propellant momentum along with their associated references is given in Table 1.

Table 1. Summary of proposed spray cone angle prediction models with additional parameters used to produce correlations for blockage factor.

Author	Correlation for θ	Additional Parameters	Flow Type	Radial Injection Type
Classical Theory	$\tan^{-1}(TMR)$	None	Not specified	Not specified
Yang et al. [1]	$(TMR)^{1/2}$	None	Not specified	Not specified
Escher [9]	$(c_1 + c_2 TMR) \cdot TMR^{1/2}$	None	Liquid-liquid	Discrete orifices
Cheng et al. [13]	$\cos^{-1}\left(\frac{1}{1 + TMR}\right)$ OR $\cos^{-1}\left(\frac{1}{1 + LMR}\right)$	None	Liquid-liquid	Annulus
Blakely et al. [7]	$a \tan^{-1}(b \cdot TMR)$	Blockage Factor	Liquid-liquid	Discrete orifices
Son [11]	$c_1 \left(\frac{TMR}{We}\right)^{c_2}$	Weber Number	Gas-liquid	Annulus
Lee [10]	$c_1 + c_2 \cdot TMR \left(\frac{H}{L_S}\right)$	Skip Distance (L_S) Orifice Height (H)	Gas-liquid	Annulus

The variety of proposed models reflects the highly empirical nature of pintle engine design. These models, however, are for a single row of orifices or a continuous annulus. While not studied for a rocket engine, investigation of mixing from multiple orifice rows has been undertaken for fuel-air combustors, focusing on the ratios of hole diameter to lateral hole spacing (within a single row), hole diameter to row spacing, and whether hole rows are aligned or staggered [21]. Although the absence of a fluid collision means these data are not directly applicable, this research points to the ratio of hole diameter to row spacing as a characteristic distance that can be used to describe the effect of multiple rows of orifices can be used for this study.

C. INJECTION CHARACTERISTICS

With the selection of a spray cone prediction model, or use of empirical studies, the geometry of the injector required to achieve the required propellant momentums can be described by incompressible fluid flow relations. Rocket engine thrust is described by a total mass flow from the engine at a given chamber pressure [22]. Therefore, it is necessary to determine the upstream pressure that will achieve that mass flow through the injector. This relationship between mass flow rate \dot{m} or volume flow rate Q and feed pressure is described by

$$\dot{m} = Q\rho = C_d A \sqrt{2\rho\Delta P} \quad (7)$$

where A is the injector element area, ρ the propellant density, ΔP the pressure drop across the element, and C_d the discharge coefficient of the injector element [22]. The discharge coefficient describes the ratio of actual mass flow to ideal mass flow if fluid were able to pass without viscous losses through the orifice, and accounts for the development of a boundary layer on the outside of A and viscous swirling that effectively reduce the velocity that can be achieved from the applied pressure difference. For momentum calculations, the average velocity from the orifice is also of interest, and is given by

$$v = \frac{\dot{m}}{\rho A} = C_d \sqrt{2\Delta P/\rho} \quad (8)$$

Using (7) and (8), the momentum of the injected flow can be determined from the pressure drop across the injector element and vice versa.

III. EXPERIMENTAL SETUP

A. INJECTOR DESIGN

The injector to be used in this study was sized for use on 1200 lbf liquid oxygen/kerosene engine. Complete high-level design parameters and the design procedure described in Appendix A produced the design point flow characteristics and pintle geometry listed in **Error! Reference source not found.** Figure 3 illustrates a cross sectional view of the injector with these parameters.

Table 2. Description of the design point characteristics selected to meet the requirements in Appendix A. Additional outputs used in component sizing are provided in Appendix A.

Fuel Mass Flow Rate [kg/s]	0.653
Oxidizer Mass Flow Rate [kg/s]	1.415
Mixture Ratio	2.20
Pintle Diameter [mm]	18.8
Number of Pintle Orifices	20
Orifice Diameter [mm]	1.59
Annulus Width [mm]	0.32

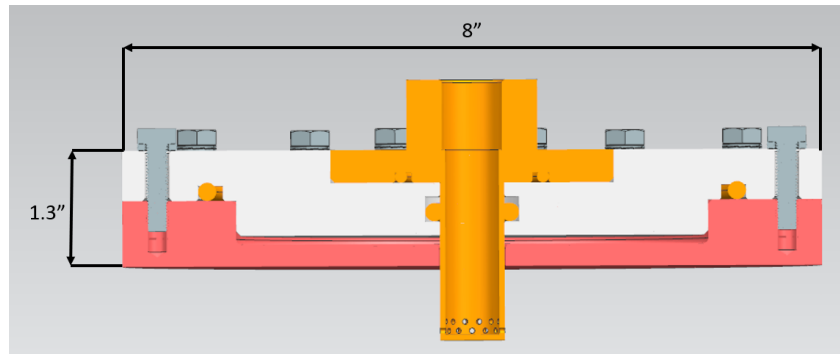


Figure 3. Cross sectional view of injector design

B. TEST MATRIX

Two quantities will be varied to accomplish the test objective: the spacing between orifice rows on the pintle and the total momentum ratio of the injected flow.

To evaluate the effect of multiple orifice rows, the 20 holes specified in Table 2 will be evenly spaced around the perimeter. The 20 holes will be split into two rows, where every other hole is the first row, and all other holes will be the second row. The two rows will be shifted vertically up and down over a succession of tests to determine ideal orifice configuration for mixing and momentum ratio. The distance between the 10 upper orifices and 10 lower orifices will be determined based on a ratio H/D_o , where H is the distance between rows of orifices, and D_o is the diameter of a single orifice as seen in Figure 4.

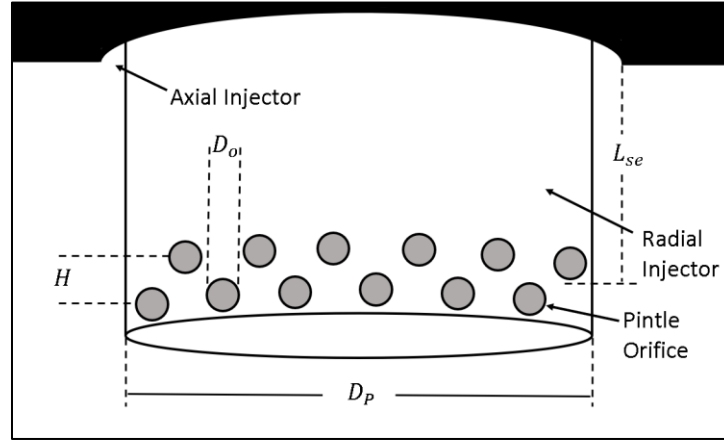


Figure 4. Pintle geometric parameters.

The experiment will use 5 pintle designs, with $H/D_o = 0, 0.5, 1, 1.5$, and 2 . Because no literature on the effects of multiple rows of orifices on pintle injectors exists, a maximum H/D_o of 2 was chosen to approximately maintain skip distance for each injector. For two rows of orifices, an effective skip distance, L_{se} , was defined as the midpoint between the two rows of orifices, as seen in Figure 4. To match the recommended skip distance for efficient combustion, effective skip distance will be set at $L_{se} = 1$, and the rows will be shifted above and below in each iteration.

To examine the formation of spray cones at different L_r/D_o , TMR is to be varied between 0.2 and 4 for each pintle geometry, corresponding with ranges examined in previous studies [2] [6] [7] [9]. To match the momentum flow of water to that of propellant of the annular and radial flows at the design point, Equations (7) and (8) can be combined as

$$\dot{m}_{H_2O} = \sqrt{\rho_{H_2O} A_{H_2O} \dot{m}_p v_p} \quad (9)$$

where the subscript H_2O indicates water flow properties and the subscript p a quantity for a propellant. To vary momentum ratio, the definition of TMR from (4) can be rewritten using (8):

$$TMR = \left(\frac{\rho_a A_a}{\rho_r A_r} \right) \left(\frac{\dot{m}_r}{\dot{m}_a} \right)^2 \quad (10)$$

The density ratios of the radial and annular flows are not matched to the ratio of densities of the propellants. However, as shown in (10), the density ratio of the axial and radial flows is included in the variation of TMR . While the viscosity and surface tension of water differs from that of the propellants as well, existing models from Table 1 indicate that water flow results are still a useful prediction of spray behavior to show the relative effect of changes in geometric parameters such as H/D_o .

Using Equations (7) and (8) with the pressure term allows calculation of the total mass flow rate and pressure drop required for each TMR combination. Because the engine components were designed with

a flight application, the mass flow rate at the design point is the maximum that can be supplied by either the pintle or annulus since a greater feed pressure would reduce margins below acceptable levels for testing. Therefore, for $TMR < 1.68$ the radial momentum through the pintle is decreased while for $TMR > 1.68$ axial momentum through the annulus must be decreased. Estimated bounding flow parameters used for the selection and design of instrumentation and setup components are listed in Table 3.

Table 3. Bounding flow conditions for water flow testing to achieve a minimum TMR of 0.2 and a maximum TMR of 4.0.

	Pintle		Annulus	
	Minimum Flow	Maximum Flow	Minimum Flow	Maximum Flow
\dot{m} [kg/s]	0.46	1.35	0.47	0.72
ΔP [kPa]	104	885	457	1073

To determine the number of tests possible without the reuse of deionized water for testing, measurement criteria were specified according to Table 4. These conditions require 3.4s flow to allow 5% of the minimum mass flow rate to collect 20g of water in the test rig. 20g of fluid was selected to ensure spray on collector walls was negligible and to provide sufficient volume to extract samples for mixing measurement. Any other TMR in the range will provide more water in the collector for the same 5% mass flow rate resolution. The available volume specified is one 55-gallon drum of deionized water from the vendor listed in the Projected Budget.

The 32 complete tests possible on a single 55 gallon of water sourced for the experiment allow 10 TMR points to be measured per H/D point tested. With two drums and capture and reuse of water using the catch basin of the test stand, sufficient water can be purchased to perform tests with reasonable uncertainty on the available budget.

Table 4. Calculation of test time and TMR testing increment based on desirable measurement parameters.

Minimum TMR	0.2
Maximum TMR	4.0
Fraction of minimum mass flow rate to be resolved	5%
Sector of spray (about engine axis) to be measured	36°
Mass required for mixture measurement	20 g
Available volume of water	0.208 m^3
Minimum test time	3.4 s
Number of tests per drum	32
Tests per H/D	10
TMR Increment	0.42

C. EXPECTED SPRAY CONE BEHAVIOR

To place and size the measurement devices used to record mass flow distribution and spray cone angle, four characteristics of the spray cone were estimated for each momentum ratio: angular span, speed, breakup distance, and droplet diameter, illustrated in Figure 5.

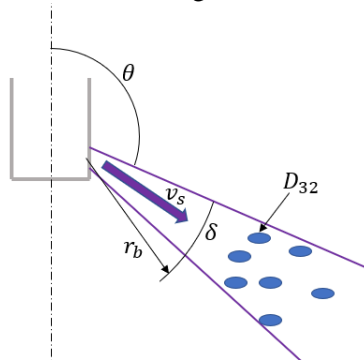


Figure 5. Illustration of angular span (δ), spray cone speed v_s , breakup distance r_b , and droplet Sauter mean diameter D_{32} .

These calculations were not intended to project test results, as angular span is the only characteristic of the four to be assessed by the experiment and because it has not been the subject of extensive research, its bounds are estimated from previous studies. Lee et al. presented a spray cone of about 20° span from patternator measurements shown in Figure 6(a) [10], and Blakely et al. presented a spray angle with an uncertainty of approximately 5° , exemplified in Figure 6(b) [7]. Son presented an empirical fit with uncertainty of approximately 6° [14]. These data indicate that an angular resolution of 4° would produce results with uncertainty comparable to existing research. In addition to mass flow distribution testing, the spread in spray cone angle will also be recorded using a DSLR camera as done in [7] and shown in Figure 6(b).

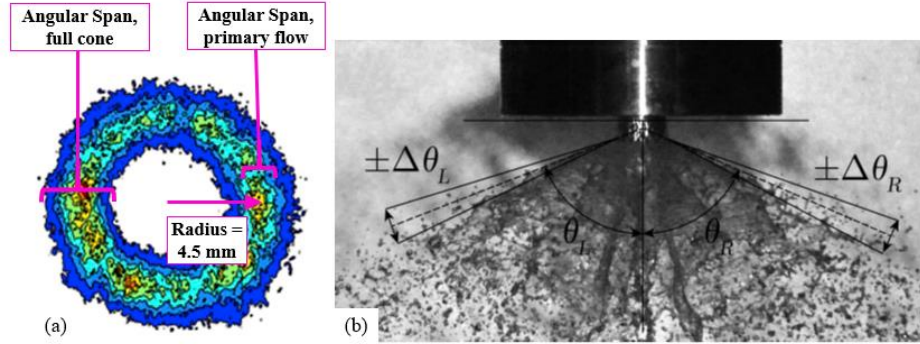


Figure 6. Results from literature used to assess angular resolution for momentum distribution study. The patternator spray image in (a) taken 7mm below the pintle tip displayed an angular span of $20 \pm 1^\circ$ and $10 \pm 1^\circ$ for the overall spray cone and primary flow, respectively [10]. The grayscale image in (b) demonstrates uncertainty $\Delta\theta$ measured for a liquid-liquid spray cone in [7].

Speed of the mixed sheet was calculated from conservation of momentum of an inelastic collision between the two fluid flows using

$$v_s = \frac{\dot{m}_a v_a + \dot{m}_r v_r}{\dot{m}_a + \dot{m}_r} \quad (11)$$

The Weber number of the sheet from (3) with the result of (11) was used to estimate breakup radius and droplet diameter. To project the droplet path, drag in the continuous sheet was assumed negligible based on spray trajectory experiments [23], and after the breakup radius a simple Euler integration program computed drag over a sphere from [24]. The breakup distance r_b – that is, the distance from the injection point where the sheet atomizes – was calculated based on the empirical relation obtained by Huang [17] for $We > 800$:

$$r_b = \frac{1}{2} d \cdot 14.2 \left(\frac{\rho_{ambient}}{\rho_{fluid}} \right)^{-2/3} We^{-1/3} \quad (12)$$

Sauter mean diameter, D_{32} , was calculated from the Weber number using the empirical relation proposed by Wu [18] and represents a droplet with the same surface-to-area ratio of the overall flow:

$$D_{32} = 133.0 \left(\frac{D_o}{8} \right) We^{-0.74} \quad (13)$$

where D_o is the orifice diameter and We is the Weber number.

Table 5. Estimates of flow behavior. Breakup distances r_b are reported to the nearest mm to correspond to manufacturing precision in the measurement apparatus described in Section III. Fluid properties used for calculation are listed in Table 9.

Flow	$We (\times 10^3)$	r_b [mm]	D_{32} [μ m]
Pintle Design: Liquid Oxygen	173	8.5	16
Pintle Test: Water	3-26	34-69	57-108
Annulus Design: Kerosene	96	8.5	25
Annulus Test: Water	13-32	32-42	57-325

While the breakup distance of the annular sheet was calculated for purposes of comparison, it was not used to inform design because the annular flow is bounded on one side by the surface of the pintle. The empirical relationship was developed for the discharge of an orifice into free space. The calculation is instead intended to serve as a qualitative comparison that the annulus and pintle breakup behaviors are expected in the same regime.

For droplets of the expected size of 57-325 μm , while the speed of the droplet decreases significantly immediately after sheet breakup, the direction of the spray changes by less than 3° , which is below the angular resolution of the measurement apparatus described below. On these droplets, drag force is much greater than gravitational force until the droplet slows significantly, shown in Figure 7. Consequently, although momentum distribution cannot be assessed because of the effects of drag on a random distribution of droplet diameters, mass flow distribution can be measured.

The engine in this investigation produces much greater thrust and chamber pressure than has been researched in previous studies [6] [7] [14] [20]. Although a pintle injector has been successfully employed on engines much larger than the 1200 lbf of this design [5], the higher chamber pressure requires a higher pressure drop across the injector to prevent backflow into the propellant feed systems from random fluctuations during firing. This results in higher flow velocities and higher Weber numbers, corresponding to more rapid sheet breakup [17] and smaller droplet diameter [25].

However, while Weber number is useful to help size the experimental setup, the higher Weber number range used in this setup should not invalidate the results. Experiments using water flow testing to compare to propellant behavior will generally exhibit Weber numbers much lower than that of the propellant itself because water features a surface tension approximately seven times greater than that of liquid oxygen with a higher density [26]. Consequently, a significantly higher flow velocity of water would be needed to match the Weber number of propellant in a combustor engine. Aside from practical issues such as increased feed pressure required to achieve this velocity, few spray cone angle models include parameters other than momentum ratio, as shown in Table 1. Moreover, within existing *TMR* studies, Weber numbers varied over multiple orders of magnitude. Thus, matching momentum flow at the design point and varying momentum ratio over the desired range is prioritized over matching Weber number.

D. TEST STAND

The injector will be mounted to a test stand to conduct the experiments outlined in this proposal. The stand has been designed and built by the USC Rocket Propulsion Laboratory (RPL) and is currently configured to support a firing of the RP-1 and liquid oxygen engine for which this injector was designed. A 3D CAD model of the test stand can be found in Appendix B, and its P&ID is detailed in Appendix C. The test stand sensor suite used to capture data is listed in Appendix D. Two orifice plates in conjunction with differential pressure transducers will be used to calculate the mass flow rate of the fluids during testing on both the fuel and oxidizer lines immediately upstream of the pintle injector. The mass flow rate measurement is given by

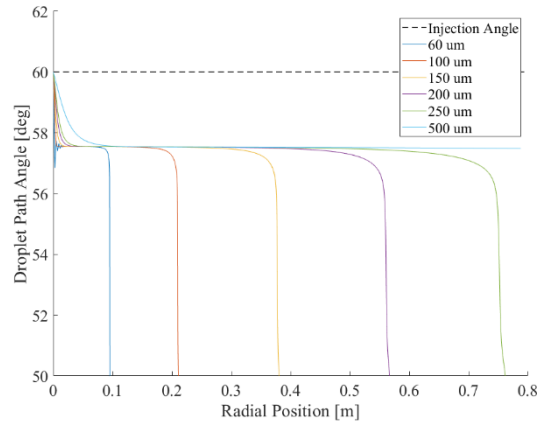


Figure 7. Angle of droplet path as a function of distance from the engine axis.

$$\dot{m} = \frac{\pi}{4} \frac{C_d}{\sqrt{1 - \left(\frac{d}{D}\right)^4}} d^2 \sqrt{2\Delta P \rho} \quad (14)$$

where d is the diameter of the orifice and D is the inlet pipe diameter upstream of the orifice [27]. Inline type K thermocouple probes will be used to determine the temperature of the fluids for density calculations.

The data acquisition unit that will be used with the test stand is a custom-built system from RPL named “microDAQ.” The unit consists of a main hub-board which is connected to a +12V power supply, a host PC, and several sidecars to support sensors. The hub PCB itself contains an STM32H743BIT6 processor. On the side of embedded software, the DAQ runs on Mbed. Since the pressure transducers on the stand vary between having VDC and mV/V electrical outputs, there are both a 5V and a millivolt sidecar to support all sensors. Both sidecars use ADS124S06 24-bit ADCs, but the millivolt sidecar also utilizes an ISL28635 differential amplifier. For thermocouple readings, the TC sidecar is equipped with MAX31856 thermocouple reader ICs and automatic cold junction compensation. By leveraging this completed infrastructure, the team will be able to easily perform tests and collect data without the additional cost or time required to assemble a new test stand.

Several initial flow tests will prepare the test stand for experimentation. To verify the orifice plate flowmeter calibration, the mass flow rate calculated from the differential pressure transducer reading will be checked against the average mass flow rate determined by the change in mass of the tanks mounted on load cells on the stand per Appendix D. With mass flow rate measurements, the discharge coefficients of the injector elements and loss coefficient of the piping system then be validated. The stand’s mass flow is controlled by the feed pressure to the water tanks, so monitoring mass flow rate as a function of feed pressure will allow these quantities to be determined to enable better control of the stand. Since mass flow rate is measured directly, these quantities will not factor into reported results, but will make testing more efficient by enabling the target TMR at each step to be more closely matched by providing appropriate upstream pressure.

To calculate uncertainty in TMR , uncertainty propagation of Equation **Error! Reference source not found.** yields

$$\frac{\Delta TMR}{TMR} = \sqrt{\left(\left(\frac{2\Delta \dot{m}_a}{\dot{m}_a}\right)^2 + \left(\frac{\Delta \rho_a}{\rho_a}\right)^2 + \left(\frac{\Delta A_a}{A_a}\right)^2\right) + \left(\left(\frac{2\Delta \dot{m}_r}{\dot{m}_r}\right)^2 + \left(\frac{\Delta \rho_r}{\rho_r}\right)^2 + \left(\frac{\Delta A_r}{A_r}\right)^2\right)} \quad (15)$$

Estimated relative uncertainties of each contributing term in (15) are listed in Table 6. Through uncertainty propagation of equation (14), \dot{m} uncertainty was calculated assuming a negligible uncertainty for the orifice plate diameter and discharge coefficient and using a differential pressure transducer with an accuracy of +/- 0.08% and pipe diameter uncertainty of +/-0.01”. Because the density of pure water at a given temperature is known within 0.001% [26], and changes negligibly with pressure uncertainty in the thermocouple of +/-0.6K is used with the rate of change of density of water with respect to temperature at 298K to calculate relative uncertainty in density. For uncertainty in annular area A_a and radial pintle injection area A_r , a machining tolerance of +/-0.025mm (0.001in) was incorporated. The calculated uncertainty in TMR of +/-4.6% produces $\Delta TMR = 0.18$ at the largest total momentum ratio of 4.0 is less than half the TMR step of 0.42 from Table 4, allowing each TMR point to be resolved separately.

Table 6. Relative uncertainties of quantities contributing to calculation of total momentum ratio.

Quantity	$\Delta x/x$ [%]
\dot{m}	0.1
ρ	0.1
A_a	4.3
A_r	1.6
TMR	4.6

E. SPRAY DISTRIBUTION TESTING RIG

The location of the mass flow rate measurement device must be located at the breakup radius to determine mass flow rate before drag on small droplets alters their path as described above. To maintain this radius at a given TMR for each catch basin, a design as shown in Figure 8 will be used.

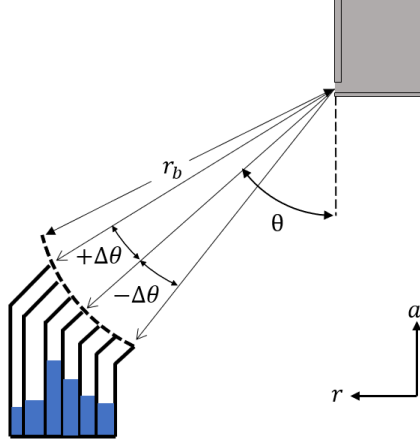
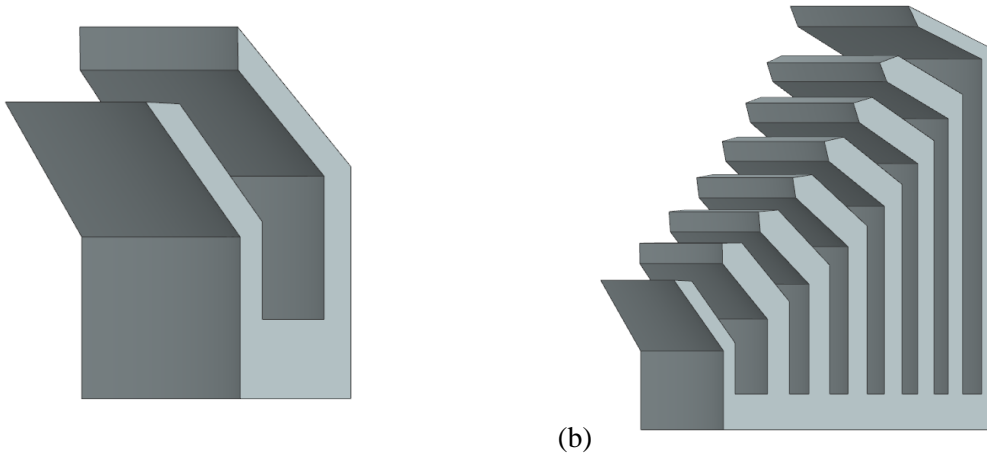


Figure 8: Experimental setup showing arrangement of catch basins for mass flow collection

The catch basins will be placed on a table made from 80/20 aluminum extrusions to ensure the basins are placed the correct distance from the pintle. The preliminary sizing of the catch basins was informed by estimations of spray behavior from Table 5. Seven individual raised containers will be aligned together providing coverage for the range $\theta = 35^\circ - 63^\circ$ with an angular resolution of 4° as discussed above. The catch basins will each cover a span of 36° in ϕ to ensure the data is not influenced by the axial location of the pintle injector; this range ensures one upper, and one lower orifice will be providing spray to the collectors. The preliminary design of these collectors is shown below in Figure 9.



(a)

(b)

Figure 9: Preliminary design of catch basins. (a) will be the smallest catch basin covering $\theta = 35^\circ - 39^\circ$. The fully assembled bank of collectors is shown in (b)

Each collector, shown in Figure 9(a), will be removable from the assembly so that its mass can be measured, ensuring that water droplets collecting on the sides of the collector are included in the measurement as well. Each basin will be manufactured from laser-cut acrylic with slotted features for assembly.

These collectors were sized to correspond to a breakup radius r_b of 77 mm, 10% higher than the maximum breakup radius predicted in Table 5. The TMR of given flow conditions affects the r_b , so extensions will be manufactured to ensure the measurement device is located for the corresponding r_b .

These will be 3-D printed and swapped out between test runs dependent on the TMR of the test. Figure 10 shows the preliminary design of these components.

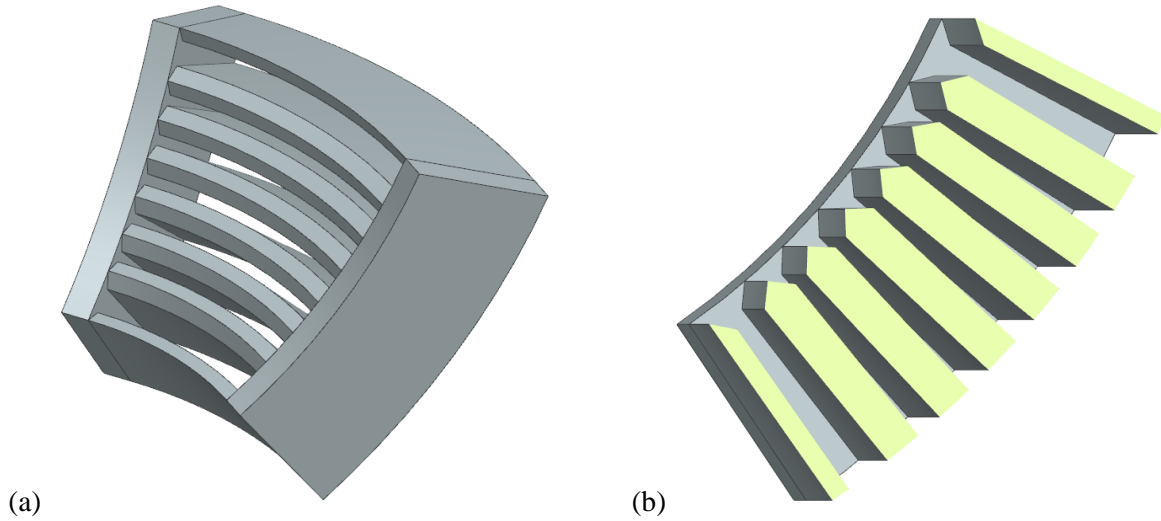


Figure 10: Preliminary design of catch basin extensions with a section view in (b). The design shown is for a r_b of 60 mm.

IV. MIXING PERFORMANCE MEASUREMENT

To evaluate the effects of L_r/D_o on mixing, a water-soluble dye will be used on the fuel line of the injector to allow traces of mixing quality to be mapped within the spread of the spray cone. A PerkinElmer Lambda 950 spectrophotometer will be used to quantify the intensity of the dye in each sample. The spectrophotometer will measure the percent transmittance of the solution with a resolution of .00007%, which is the percentage of light which passes through a sample, representing the saturation of dye in a sample of water [28]. Samples of the test fluid in the fuel line and of pure deionized water will be taken to provide reference percent transmittance measurements. The water flow test will then be run, spraying the mixed flows into the catch basins described above. The transmissivity of each sample from each angular bin will then be measured by the spectrophotometer. The fraction of water originating from the pintle and annulus flows can be determined from the diluted dye concentration in the sample calculated from the reference transmissivities of the unmixed pintle and annular flows. From this the mixing quality measured in each catch basin, a discretized model can be made representing mixing quality over the angular span of the spray. With this model, it can be determined if there is a relationship between pintle geometry and uniformity of mixing. This analysis will be done with the goal of seeking which pintle configuration creates the most uniform mixing over the entire spread of the spray cone, and if any relationship can be drawn between geometry and quality of mixing.

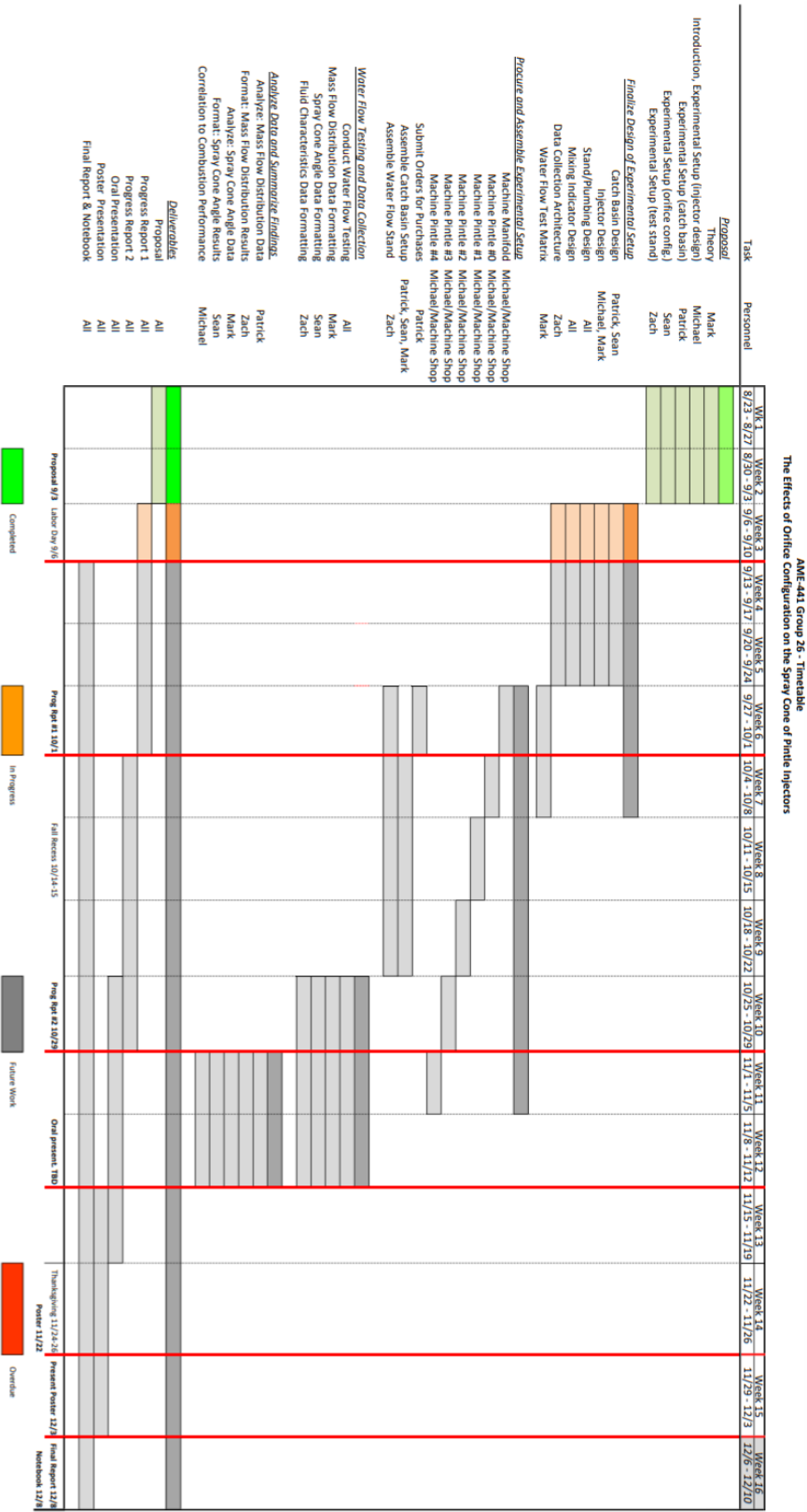
V. CONCLUSION

In the preceding sections, the concept of pintle orifice configuration, the motivation for study, and proposed testing procedure were presented. This study will look at how the non-dimensional ratio H/D of the space between orifice rows H and the orifice diameter D_o affect the performance of a pintle rocket engine injector. To evaluate the effect of H/D , the spray cone angle θ and mass flow distribution will be examined over a range of momentum ratios. This will be accomplished through a measurement device that collects water in catch basins for discretized θ ranges. The quality of mixing in this experiment will also be evaluated using dyed water in the annular flow. Spectrophotometer measurements of the final color composition of the flow for each catch basin will determine if fluid from the annular and radial flows is consistent through different spray cone angles. Gathering this information will enable the characterization of the effect H/D_o on the performance of a pintle injector, allowing selection of injector geometry that can maximize flow rate and provide a desired combustion distribution for a given chamber.

VI. COST ESTIMATE

AME-441 Group 26 - Cost Estimate								
THE EFFECTS OF ORIFICE CONFIGURATIONS ON THE SPRAY CONE ANGLE OF A PINTLE INJECTOR								
as of 9/3/2021								
				Vendor/Manufacturer	Model/Part No.	Qty.	Unit Price	Item Price
EXPENSES FOR ITEMS AVAILABLE IN LAB								
Equipment								
	High Speed Camera			Kron	Chronos 1.4	1	\$3,774.00	\$3,774.00
	Spectrophotometer - Dornsife Dept. of Chemistry: https://dornsife.usc.edu/chemistry/			Perkin-Elmer	UV-Vis-NIR	1	\$5,000.00	\$5,000.00
	RPL Liquids Test Stand			USC RPL	N/A	1	\$29,450.36	\$29,450.36
	3-D Printer			Prusa Research	PRI-MK3S-KIT-ORG-PEI	1	\$999.00	\$999.00
	Laser Cutter			Universal Laser Systems	M300	1	\$5,000.00	\$5,000.00
Materials								
	Al-6061 8.5" D, 6" L Cylindrical Stock			McMaster Carr	8974K901	1	\$348.87	\$348.87
	Al-6061 4" D, 6" L Cylindrical Stock			McMaster Carr	89774K97	5	\$70.04	\$350.20
	1/4-28 x 1" Grade 8 Bolts			McMaster Carr	92620A564	1	\$9.79	\$9.79
	1/4" Nordlock Washers			McMaster Carr	91812A229	4	\$9.62	\$38.48
	1/4" Thick Acrylic Sheet 12" x 24"			McMaster Carr	8589K82	1	\$19.14	\$19.14
	1/16" Thick Acrylic Sheet 24" x 48"			McMaster Carr	8589K14	1	\$34.79	\$34.79
	Prusament PLA Filament, 1 kg			Prusa Research	PRM-PLA-JET-1000	1	\$24.99	\$24.99
Manufacturing								
	Turning (\$70 per hour)			AME-441/RPL Machine Shop	DWG-GRP-26-01R1	70	\$70.00	\$4,900.00
	Milling (\$70 per hour)			AME-441/RPL Machine Shop	DWG-GRP-26-02R1	50	\$70.00	\$3,500.00
	Laser Cutting (\$40 per hour)			AME-441 Machine Shop	DWG-GRP-26-03R2	3	\$40.00	\$120.00
							Sub-total Cost:	\$53,569.62
EXPENSES FOR ITEMS REQUIRED FOR PURCHASE								
Equipment								
	55 Gallon Drum - Industrial Distilled Water			Puritan Springs		2	\$71.40	\$142.80
	Water-Soluble Blue Dye			McMaster Carr	1347N12	2	\$48.95	\$97.90
Materials								
	Silicone Oring (-222)			McMaster Carr	9396K82	1	\$5.67	\$5.67
	Silicone Oring (-313)			McMaster Carr	9396K284	1	\$11.23	\$11.23
	Silicone Oring (-330)			McMaster Carr	9396K298	1	\$11.04	\$11.04
	Epoxy, J-B Weld Clearweld, 8 oz. Syringe			McMaster Carr	7605A23	2	\$24.14	\$48.28
	T-Slotted Framing (1010 8020) (10ft L)			McMaster Carr	47065T101	2	\$33.18	\$66.36
	T-Slotted Frame Nuts (1/4-20)			McMaster Carr	47065T905	2	\$5.44	\$10.88
	Button Head Screw 1/4"-20 x 0.5"			McMaster Carr	92949A537	1	\$5.57	\$5.57
	T-Slotted Frame Corner Brackets			McMaster Carr	47065T239	15	\$5.68	\$85.20
							Sub-total Cost:	\$484.93
							TOTAL PROJECT EXPENSES:	\$54,054.55
BUDGET								
	AME-441 project budget (\$100 per student)					5	\$100.00	\$500.00
							TOTAL BUDGET:	\$500.00

VII. TIMETABLE



VIII. REFERENCES

- [1] V. Yang, M. Habiballah, J. Hulka and M. Popp, *Liquid Rocket Thrust Chambers: Aspects of Modeling, Analysis, and Design*, Reston: American Institute of Aeronautics and Astronautics, 2004.
- [2] B. Austin, S. Heister and W. Anderson, "Characterization of Pintle Engine Performance for Nontoxic Hypergolic Bipropellants," *J. Propulsion and Power*, vol. 21, no. 4, pp. 627-635, 2005.
- [3] W. Carter and G. Bell, "Development and Demonstration of a N₂O₄/N₂H₄ Injector," Air Force Rocket Propulsion Laboratory, Redondo Beach, 1969.
- [4] X.-x. Fang and C.-b. Shen, "Study on atomization and combustion characteristics of LOX/methane pintle injectors," *Acta Astronautica*, vol. 136, pp. 369-379, 2017.
- [5] G. Dressler and J. Bauer, "TRW Pintle Engine Heritage and Performance Characteristics," American Institute of Aeronautics and Astronautics, Redondo Beach, 2000.
- [6] R. Rezende, A. Pimenta and V. d. C. Perez, "Experiments with Pintle Injector Design and Development," in *Propulsion and Energy Forum*, Orlando, 2015.
- [7] J. Blakely, J. Freeberg and J. Hogge, "Spray Cone Formation from Pintle-Type Injector Systems in Liquid Rocket Engines," University of Southern California, Los Angeles, 2017.
- [8] P. Cheng, Q. Li, S. Xu and Z. Kang, "On the prediction of spray angle of liquid-liquid pintle injectors," *Acta Astronautica*, vol. 138, pp. 145-151, 2017.
- [9] D. W. Escher, "Design and Preliminary Hot Fire and Cold Flow Testing of Pintle Injectors," Pennsylvania State University, 1996.
- [10] S. Lee, D. Kim, J. Yoo and Y. Yoon, "Spray characteristics of a pintle injector based on annular orifice area," *Acta Astronautica*, vol. 167, pp. 201-211, 2020.
- [11] M. Son, K. Yu, J. Koo, O. C. Kwon and J. S. Kim, "Effects of Momentum Ratio and Weber Number on Spray Half Angles of Liquid Controlled Pintle INjector," *J. Thermal Science*, vol. 24, no. 1, pp. 37-43, 2015.
- [12] T. Mueller, "Pintle Injector Tip with Active Cooling". United States Patent 7,503,511, 17 March 2009.
- [13] P. Cheng, Q. Li and H. Chen, "Flow characteristics of a pintle injector element," *Acta Astronautica*, vol. 154, pp. 61-66, 2019.
- [14] M. Son, K. Radhakrishnan, J. Koo, O. C. Kwon and H. D. Kim, "Design Procedure of a Movable Pintle Injector for Liquid Rocket Engines," *J. Propulsion and Power*, vol. 33, no. 4, pp. 858-869, 2017.

- [15] B. Wang, T. Badawy, Y. Jiang, H. Xu, A. Ghafourian and X. Zhang, "Investigation of deposit effect on multi-hole injector spray characteristics and air/fuel mixing process," *Fuel*, vol. 191, pp. 10-24, 2017.
- [16] S. Lee, J. Koo and Y. Yoon, "Effects of skip distance on the spray characteristics of a pintle injector," *Acta Astronautica*, vol. 178, pp. 471-480, 2021.
- [17] J. Huang, "The break-up of axisymmetric liquid sheets," *J. Fluid Mech*, vol. 43, no. 2, pp. 305-319, 1970.
- [18] P. Wu, L. Tseng and G. Faeth, "Primary Breakup in Gas/Liquid Mixing Layers for Turbulent Liquids," *Atomization and Sprays*, vol. 2, pp. 295-317, 1992.
- [19] R. Luna and W. Klimoff, "On Aerodynamic Breakup of Liquid Drops," Sandia Laboratories, Livermore, 1967.
- [20] S. Ninish, A. Vaidyanathan and K. Nandakumar, "Spray characteristics of liquid-liquid Pintle injector," *Experimental Thermal and Fluid Science*, vol. 97, pp. 324-340, 2018.
- [21] J. Holdeman, "Mixing of Multiple Jets with a Confined Subsonic Crossflow," *Prog. Energy Combust. Sci.*, vol. 19, pp. 31-70, 1993.
- [22] G. Sutton and O. Biblarz, *Rocket Propulsion Elements*, 9th ed., Hoboken: Wiley, 2017.
- [23] B. Trettel and O. Ezekoye, "Theoretical Range and Trajectory of a Water Jet," in *International Mechanical Engineering Congress and Exposition*, Houston, 2015.
- [24] F. Morrison, "Data Correlation for Drag Coefficient for a Sphere," Michigan Technological University, Houghton, 2016.
- [25] W. Nurick, "Orifice Cavitation and Its Effect on Spray Mixing," *J. Fluids Eng.*, vol. 98, no. 4, pp. 681-687, 1976.
- [26] E. Lemmon, M. McLinden and D. Friend, "Thermophysical Properties of Fluid Systems," in *NIST Chemistry WebBook, NIST Standard Reference Database Number 69*, National Institute of Standards and Technology, 2021.
- [27] "Orifice, Nozzle and Venturi Flow Rate Meters," The Engineering ToolBox, 2004. [Online]. Available: https://www.engineeringtoolbox.com/orifice-nozzle-venturi-d_590.html. [Accessed 3 9 2021].
- [28] PerkinElmer, "PerkinElmer.com," 2004. [Online]. Available: https://resources.perkinelmer.com/lab-solutions/resources/docs/BRO_Lambda950850650Americas.pdf. [Accessed 3 September 2021].
- [29] D. Huzel and D. Huang, *Design of Liquid Propellant Rocket Engines*, Washington, D.C.: National Aeronautics and Space Administration, 1967.

- [30] Y. Cengel and A. Ghajar, Heat and Mass Transfer, 5th ed., New York: McGraw Hill Education, 2015.
- [31] S. Lambiris and L. Combs, "Steady-state Combustion Measurements in a LOX/RP-1 Rocket Chamber and Related Spray Burning Analysis," in *Detonation and Two-Phase Flow*, New York, Academic Press Inc., 1962, pp. 269-304.
- [32] W. Penttermann and W. Wagner, "New pressure-density-temperature measurements and new rational equations for the saturated liquid and vapour densities of oxygen," *J. Chem. Thermodynamics*, vol. 10, no. 12, pp. 1161-1172, 1978.
- [33] B. McBride and S. Gordon, "Computer Program for Calculation of Complex Chemical Equilibrium Compositions and Applications," National Aeronautics and Space Administration, Cleveland, 1996.
- [34] B. Vasques and O. Haidn, "Effect of Pintle Injector Element Geometry on Combustion in a Liquid Oxygen/Liquid Methane Rocket Engine," in *European Conference for Aeronautics and Aerospace Sciences*, Milan, 2017.
- [35] B. Munson, D. Young, T. Okiishi and W. Huebsch, Fundamentals of Fluid Mechanics, Hoboken: Wiley, 2009.
- [36] W. Hammock, E. Currie and C. Fisher, "Apollo Experience Report - Descent Propulsion System," National Aeronautics and Space Administration, Houston, 1973.
- [37] Lewis Research Center, "Liquid Rocket Engine Injectors," National Aeronautics and Space Administration, Cleveland, 1976.
- [38] J. Cherne, "Mechanical Design of the Lunar Module Descent Engine," Redondo Beach, 1967.
- [39] T. Ohrn, D. Senser and A. Lefebvre, "Geometrical Effects on Discharge Coefficients for Plain-Orifice Atomizers," *Atomization and Sprays*, vol. 1, no. 2, pp. 137-153, 1991.
- [40] M. Weinzierl, "Space, the Final Economic Frontier," *J. Econ. Perspectives*, vol. 32, no. 2, pp. 173-192, 2018.
- [41] M. Weinzierl, K. Lucas and M. Sarang, *SpaceX, Economies of Scale, and a Revolution in Space Access*, Boston: Harvard Business School, 2020.
- [42] K. Sakaki and et al., "Performance Evaluation of Rocket Engine Combustors using Ethanol/Liquid Oxygen Pintle Injector," in *52nd AIAA/SAE/ASEE Joint Propulsion Conference*, Salt Lake City, 2016.

IX. APPENDICES

APPENDIX A: ENGINE HIGH-LEVEL DESIGN PARAMETERS

The injector used in this investigation was sized for an engine intended for a small, student-built flight vehicle. As a result, a limited range of composite materials and metals were available, with the use only of manual machines an additional constraint on possible geometries. Thrust and firing time were estimated from performance goals for the vehicle. Chamber pressure was maximized for from the thickness of the combustion chamber wall possible in a layup, minus expected ablation [29] and with a factor of safety of 2. The pressure drop across the injector elements was selected to provide at least 25% of chamber pressure to prevent intrusion of combustion products into the injector, while the upper bound was determined by the capabilities of an upstream piping system in development for a hot firing.

Table 7. High-level design requirements for the engine design used as a test subject in this experiment.

Fuel	RP-1/Jet-A
Fuel Temperature	300 K
Oxidizer	Liquid Oxygen
Oxidizer Temperature	100 K
Thrust	1200 lbf
Firing Time	15 s
Chamber Pressure	400 psi
Nozzle Exit Pressure	57.2 kPa
Element Pressure Drop Range at Nominal Flow conditions	$100 \text{ psi} \leq \Delta P \leq 150 \text{ psi}$

Using these parameters, a NASA CEA analysis was used to optimize mixture ratio by meeting the required parameters with minimal mass flow rate. These results and the chamber fluid properties used to dimension the nozzle and inform heat transfer analyses, are presented in Table 8.

Table 8. Chamber parameters for the engine design used as a test subject in this experiment based on the design requirements in Table 7 and CEA analysis.

Chamber Temperature	3517 K
Fuel Mass Flow Rate	0.653 kg/s
Oxidizer Mass Flow Rate	1.415 kg/s
Oxidizer/Fuel Ratio	2.2
Chamber Temperature	3517 K
Specific Gas Constant	378.1
Specific Heat Ratio	1.164

To appropriately specify geometric parameters for the measurement apparatus and the injector using Equations (7) and (8), the discharge coefficient and expected droplet diameter produced by the pintle orifices needed to be calculated. The discharge coefficient calculation followed the algorithm developed by Nurick et al. to check for cavitation, using the properties for liquid oxygen and water given in Table 9 [25].

Table 9. Inputs and outputs of discharge coefficient calculation. Except where indicated, sources are [26] for liquid oxygen and [30] for liquid water. The droplet diameter is calculated for a flow of water with equal momentum to the flow of liquid oxygen to be used during firing.

Property	Design: Liquid Oxygen, 100K	Test: Water, 300 K
ρ [kg/m ³]	1088	998
μ [kg/m/s]	1.526×10^{-4}	1.002×10^{-3}
P_{vap} [Pa]	253180	2339
σ [N/m]	0.0108	0.0717

C_d	0.815	0.857
v [m/s]	30.03 (calculated using (3))	31.36 (calculated using (3))

The values calculated for liquid oxygen were used for the design of the injector, while the discharge coefficient of the injector for water was used to inform the pressure drop calculations presented in Section III. Using guesses at orifice diameter from initial runs, liquid oxygen droplet diameter calculated per Equation (13) and was iteratively confirmed as the final geometry was selected. Charts from [31] allowed estimation of combustion time for a droplet of this size as 0.001s.

With projected combustion behavior, Equation (7) and (11) were used to approximately place the flame from the spray cone based on a set of manufacturing inputs. The set of outputs meeting design requirements and placing the combustion region in a preferred location for heat distribution led to the geometry selection provided in Table 10, with the corresponding output selection in Table 11. Although only one combination is shown, the program iterated through thousands of possibilities to optimize the result.

Table 10. Inputs for simplified injector sizing function. Except for C_d , \dot{m} , and ρ , all parameters were varied to examine geometries over a range of geometric inputs. The values shown are for the selected geometry combination used in testing.

Input	Oxidizer (Pintle)	Fuel (Annulus)
C_d	0.815 (Calculated – see below)	0.9 [29]
\dot{m} [kg/s]	1.415 (Table 8)	0.653 (Table 8)
ρ [kg/m ³]	1088 [32]	818 [33]
d_p [mm]	18.80	
τ_p [mm]	2.78	
N [number of holes]	20	
d_h [mm]	1.98	
$w_{annulus}$ [mm]	0.343	

Table 11. Outputs of simplified injector sizing function. The values shown are for the selected geometry combination presented in Table 10. Many combinations were considered before this was selected.

Output	Oxidizer (Pintle)	Fuel (Annulus)
v [m/s]	30.03	38.71
ΔP [MPa]	0.739	0.757
Estimated Combustion Distance from Pintle [mm]	54	

APPENDIX B: USC RPL Liquids Test Stand 3D CAD Model

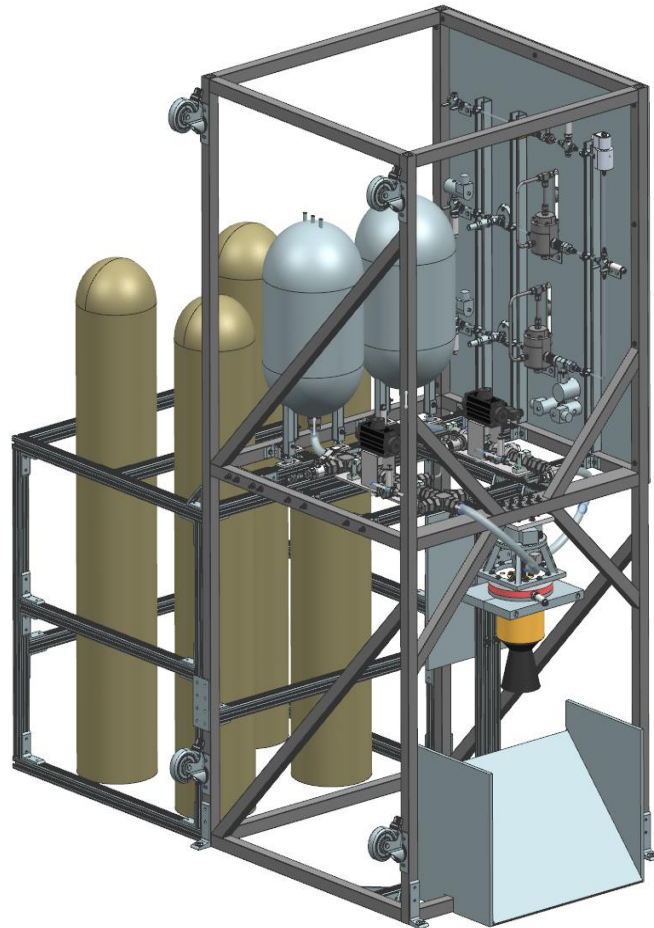


Figure 11. USC RPL “Freezer Burn” Liquids Test Stand CAD Model

APPENDIX C: USC RPL Liquids Test Stand P&ID

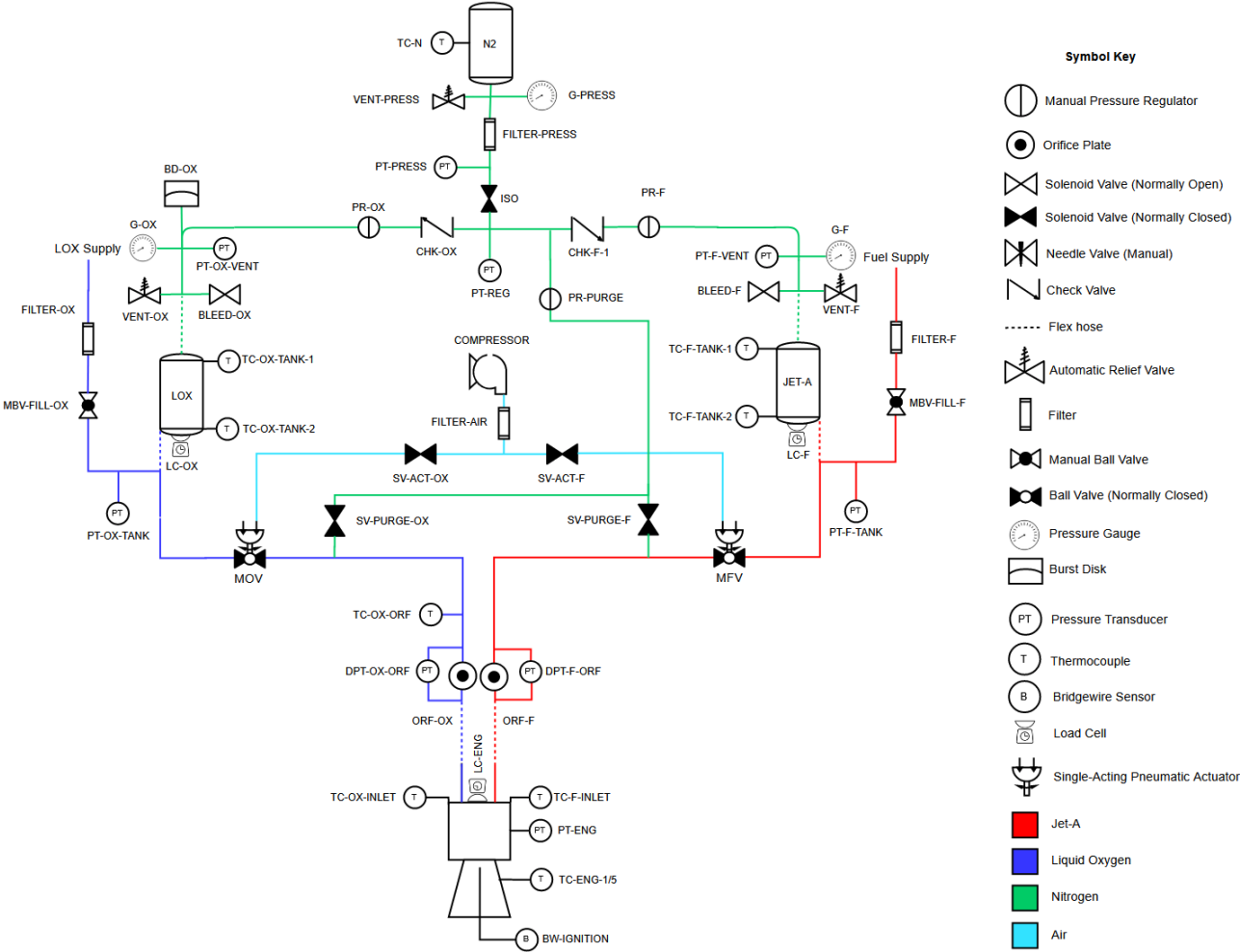


Figure 12. USC RPL “Freezer Burn” Liquids Test Stand P&ID

APPENDIX D: USC RPL Liquids Test Stand Sensors List

Table 12. List of all sensors on the USC RPL “Freezer Burn” Liquids Test Stand. Sensors bolded will be used for direct calculations. All other sensors are purposed for general system data collection and control.

Sensor Type	P&ID P/N	Measurement	Output	Model #
Pressure Transducers	PT-PRESS	Nitrogen Tank Pressure	0-5 Vdc	PX329-3KG5V
	PT-REG	Regulator Pressure	0-5 Vdc	PX329-3KGV
	PT-OX-VENT	LOX side Vent Pressure	10 mV/V	PX329-1KGV
	PT-F-VENT	Kerosene side Vent Pressure	10 mV/V	PX329-1KGV
	PT-OX-TANK	LOX Tank Pressure	0-5 Vdc	PX329-1KGV
	PT-F-TANK	Kerosene Tank Pressure	0-5 Vdc	PX329-1KGV
	DPT-OX-ORF	LOX side Orifice Plate Differential Pressure	10 mV/V	PX409-250DWUV
	DPT-F-ORF	Kerosene side Orifice Plate Differential Pressure	10 mV/V	PX409-250DWUV
	PT-ENG	Engine Pressure	10 mV/V	PX329-1KGV
Load Cells	LC-OX-1	LOX Tank Weight	2 mV/V	ASIN B077YHNNCP
	LC-OX-2	LOX Tank Weight	2 mV/V	ASIN B077YHNNCP
	LC-OX-3	LOX Tank Weight	2 mV/V	ASIN B077YHNNCP
	LC-F-1	Kerosene Tank Weight	2 mV/V	ASIN B077YHNNCP
	LC-F-2	Kerosene Tank Weight	2 mV/V	ASIN B077YHNNCP
	LC-F-3	Kerosene Tank Weight	2 mV/V	ASIN B077YHNNCP
	LC-ENG	Engine Axial Thrust	3 mV/V	Honeywell Model 41: 060-0574-03
Thermocouples	TC-N	Nitrogen Tank Temperature	mV	SA1-K-SRTC
	TC-OX-TANK-1	LOX Tank Temperature	mV	SA1-K-SRTC
	TC-OX-TANK-2	LOX Tank Temperature	mV	SA1-K-SRTC
	TC-F-TANK-1	Kerosene Tank Temperature	mV	SA1-K-SRTC
	TC-F-TANK-2	Kerosene Tank Temperature	mV	SA1-K-SRTC
	TC-OX-ORF	LOX side Orifice Plate Temperature	mV	SA1-K-SRTC
	TC-F-ORF	Fuel side Orifice Plate Temperature	mV	SA1-K-SRTC
	TC-ENG-1	Engine/Nozzle Temperature	mV	SA1-K-SRTC
	TC-ENG-2	Engine/Nozzle Temperature	mV	SA1-K-SRTC
	TC-ENG-3	Engine/Nozzle Temperature	mV	SA1-K-SRTC
	TC-ENG-4	Engine/Nozzle Temperature	mV	SA1-K-SRTC
	TC-ENG-5	Engine/Nozzle Temperature	mV	SA1-K-SRTC

